Stability and Folding/Unfolding Kinetics of the Homotrimeric Coiled Coil Lpp-56†

Saša Bjelić,‡ Andrey Karshikoff,§ and Ilian Jelesarov*,‡

Biochemisches Institut der Universität Zürich, Winterthurerstr. 190, CH-8057 Zürich, Switzerland, and Department of Biosciences and Nutrition, Karolinska Institute, Stockholm, Sweden

Received April 26, 2006; Revised Manuscript Received May 29, 2006

ABSTRACT: The 56 amino acid long protein moiety of the *E. coli* outer membrane lipoprotein (Lpp-56) contains a 4,3 hydrophobic heptad repeat and forms a parallel, in-register trimeric coiled coil in solution. The unconventional structural properties of Lpp-56 make it an interesting experimental object to study the folding of a trimeric coiled coil. Folding is unusually slow at low temperatures, and the rates of folding and unfolding are balanced in such a way that the thermodynamic equilibrium is established after considerable time at high temperatures or in the presence of denaturants. Here, we examine the stability and the folding/unfolding kinetics of Lpp-56 at neutral pH using GdmCl as the denaturant. Folding and unfolding appear to represent structural transitions between the folded trimer and the unfolded monomer, without detectable intermediates. For the first time, we estimated the unfolding free energy from a direct measurement at equilibrium. Our estimate of $\Delta G_U = 79 \pm 10$ kJ mol^{-1} compares very well with $\Delta G_U \sim 76-88$ kJ mol^{-1} obtained from the kinetic rate constants of refolding (7×10^5 M^{-2} s^{-2}) and unfolding (10^{-9} to 10^{-11} s^{-1}) and is almost half of the ΔG_U recently suggested using a different methodology (Dragan, A. I., Potekhin, S., Sivolob, A., Lu, M., and Privalov, P. L. (2004) *Biochemistry 43, 14891−14900*). Because GdmCl attenuates electrostatic interactions, the discrepancy can be partly explained by an electrostatic component of the unfolding barrier. The combined information illustrates the difficulties in obtaining a precise biophysical description of proteins that exhibit unusual kinetic properties. Lpp-56 is the first coiled coil for which a high unfolding kinetic barrier has been experimentally demonstrated.

Our current knowledge about the energetics and kinetics of protein folding originates mainly from studies of monomeric protein domains. However, oligomeric proteins are in fact more abundant in nature, as the consequence of a strong evolutionary pressure for monomers to associate into oligomers (*1*). Folding of monomers and oligomers is driven by the same type of noncovalent interactions and thermodynamic principles. In oligomers, the forces stabilizing and destabilizing the natively folded structure operate not only within the single subunit but also between the subunits. Furthermore, the formation of an oligomeric protein includes at least one concentration-dependent step because folding and association are often tightly coupled processes. If the subunits are completely (or almost completely) unstructured in isolation, the 3D structure is maintained through intersubunit interactions. The thermodynamics and folding mechanism of relatively short, dimeric α-helical coiled coils being archetypal for this class of oligomers have been studied in considerable detail (*2*). Much less is known about the energetics and kinetics of trimeric and higher order oligomeric coiled coils.

The Braun's lipoprotein (Lpp) is the most abundant protein in the *E. coli* outer membrane. It exists in a free form and in a bound form, which is covalently linked to the peptidoglycan matrix. Lpp is a major player in maintaining the architecture and function of the outer membrane. The 56 amino acid long protein moiety of Lpp (Lpp-56[1]) contains a 4,3 hydrophobic heptad repeat and forms a parallel, in-register trimeric coiled coil in solution (*3*). The crystal structure of Lpp-56 exhibits intriguing peculiarities: (i) an intricate, water-mediated hydrogen-bonding network firmly anchors an umbrella-shaped capping structure at the *N*-terminal. (ii) The three *C*-terminal tyrosine rings form well-defined van der Waals contacts with 3-fold symmetry. Both structural motifs appear to fix and stabilize the termini of the coiled coil, which are flexible and fraying in many other coiled coils. (iii) Three successive *a* and *d* layers include alanine residues. (iv) β-Branched residues (Val, Ile) predominantly occupy the *a* positions, and nonbranched residues (Leu, Ala, Met) exclusively occupy the *d* positions, in contrast to all other trimeric coiled coils known. (v) Finally, the supercoil radius of the alanine-zipper region is 5.2 Å instead of 6.7 Å in a regular three-stranded coiled coil. As a result, Lpp-56 exhibits unique α-helical curvature. The unconventional structural properties of Lpp-56 make it an interesting experimental object to study the folding of a trimeric coiled coil.

† This work was supported in part by the Swiss National Science Foundation (grant 31-100197/1).

* To whom correspondence should be addressed. Phone: ++41 44 635 5547. Fax: ++41 44 635 6805. E-mail: iljel@bioc.unizh.ch.

‡ Biochemisches Institut der Universität Zürich.

§ Karolinska Institute.

[1] Abbreviations: ΔC_p, heat capacity change; f_U, molar fraction of unfolded protein; $\Delta G_U^{H_2O}$, unfolding free energy; k_f, refolding rate constant; k_u, unfolding rate constant; Lpp-56, the protein moiety of the outer membrane lipoprotein of *E. coli*; LEM, linear extrapolation method; m_{eq}, the first derivative of the observed unfolding free energy with respect to the denaturant concentration; m_f and m_u, the first derivatives of the logarithm of the folding rate constant and unfolding rate constant, respectively, with respect to the denaturant concentration; MRE_{225}, mean residue ellipticity at 225 nm.

10.1021/bi0608156 CCC: $33.50 © 2006 American Chemical Society
Published on Web 07/01/2006

A couple of years ago, we initiated a thermodynamic and kinetic investigation of Lpp-56 at pH 5, where thermal unfolding is completely reversible (see Supporting Information for some results of this study). We realized that folding is unusually slow at low temperatures, and the rates of folding and unfolding are balanced in such a way that the equilibrium between the folded trimer and the unfolded monomer is established after considerable time at high temperatures or in the presence of denaturants. As it sometimes happens in research, while our studies were in an advanced stage, Dragan et al. published an extensive study on the biophysics of Lpp-56-folding at neutral pH (*4*). (Henceforth, we refer to this work as DP, acknowledging the first and the principal authors). They presented a wealth of data documenting well the kinetic peculiarity of the protein. DP used an innovative and elegant method to derive information on the energetics of the folded state from experiments performed under nonequilibrium conditions and provided insights into the energetics of the folding transition state. One important conclusion of this study is that the free energy of unfolding at 4 °C amounts to 137 kJ mol^{-1}, corresponding to an unfolding equilibrium constant of 1.5×10^{-26} M^2. Because the directly measured rate constant of folding at 5 °C was 2.3×10^6 M^{-2} s^{-1} and both folding and unfolding could be modeled with simple 3M → T and T → 3M reactions, respectively, the rate constant of unfolding should be on the order of 10^{-20} s^{-1} at benign conditions. It follows that the expected half time for Lpp-56 unfolding is on the order of 10^{12} years!

Intrigued by this extremely high kinetic stability, here we reexamine the stability and the folding/unfolding kinetics of Lpp-56 at neutral pH using GdmCl as the denaturant. For the first time, we estimated the unfolding free energy from a direct measurement at equilibrium. Our estimate of $\Delta G_U = 79 \pm 10$ kJ mol^{-1} compares very well with the $\Delta G_U \sim 76-88$ kJ mol^{-1} obtained from the kinetic rate constants of refolding and unfolding and is almost half of the ΔG_U suggested by DP using a different methodology. The discrepancy can be partly explained by an electrostatic component of the unfolding barrier. The combined information illustrates the difficulties in obtaining a precise biophysical description of proteins that exhibit unusual kinetic properties.

EXPERIMENTAL PROCEDURES

The Lpp-56 protein was provided by Dr. Min Lu from Cornell University. The expression and purification procedures were described (*3*). The sequence of the protein is given in Figure S2 of Supporting Information. The purity of the protein was checked by RP-HPLC, and the mass was verified by mass spectroscopy. Protein monomer concentration was determined by measuring UV absorbance at 280 nm in 6 M GdmCl using an extinction coefficient $\epsilon = 1280$ M^{-1} cm^{-1} calculated from the amino acid sequence (*5*). Concentrated stock solutions were prepared by dissolving the lyophylized protein either in an aqueous buffer or in a buffer containing 6 M GdmCl and by performing extensive dialysis for at least 20 h.

Buffer. All experiments were conducted in a standard PBS buffer (8.3 mM Na_2HPO_4, 1.47 mM KH_2PO_4, 137 mM NaCl, 2.7 mM KCl; I = 164 mM) at pH 7.0. The pH of buffers containing GdmCl was adjusted after adding the denaturant. The GdmCl concentration of each sample was verified by measuring the refractive index.

Circular Dichroism (CD) Spectroscopy. Equilibrium unfolding experiments were performed on a Jasco-715 instrument (Jasco Ltd.), the calibration of which was routinely checked. In addition, for manual mixing kinetic experiments, models J-500 and J-810 were used. All spectrometers were equipped with a computer-controlled water bath. Cylindrical jacketed cuvettes of 0.1 and 1.0 cm spectral paths were used.

Equilibrium Unfolding Experiment. The final protein concentration concentration of all samples was 12 μM (monomer equivalents) in PBS containing 0−6 M GdmCl. The protein was diluted from stock solutions prepared in either PBS or PBS containing 6 M GdmCl. Each solution was split into aliquots and stored at 4 °C in sterile tubes to prevent contamination during the experiment. Extreme care was taken not to disturb the thermal equilibrium during the measurement. The solutions were transferred using chilled pipet tips directly into the cuvette, which had been mounted in the cell-holder and extensively prethermostated. The ellipticity at 225 nm was sampled for 3 min after complete thermal equilibration and averaged over 60 data points. As a test for possible instrumental drift samples in which the equilibrium was established after a few days of incubation, were regularly remeasured. No systematic instrumental drift was detected.

Manual Mixing Kinetics. Depending on the protein concentration and GdmCl concentration, the apparent half times of folding and unfolding of Lpp-56 range from seconds to hours to days to months. The time course of the ellipticity change at 225 nm was used to follow the refolding/unfolding reactions at 4 °C. Slow unfolding kinetic traces (half times >200 s) were monitored upon the manual mixing of the folded protein with the buffer containing GdmCl to achieve the desired final protein concentration and the desired final denaturant concentration (typically 30 μM Lpp-56 monomer and 3−4 M GdmCl). For monitoring the folding kinetics, the protein was denatured by incubation for 4 min at 80 °C or in 6 M GdmCl at 4 °C. The folding reaction was initiated either by transferring the heat-denatured protein directly into the prethermostated cuvette mounted in the cell-holder of the spectropolarimeter or by rapid dilution into the prechilled buffer without GdmCl. The dead time of manual mixing was always <20 s, much shorter than the half time of the reaction under study. The temperature variation during manual mixing was estimated to be not larger than ±1 °C, and thermal equilibrium was established after about 3 min. The data were collected every 1 s in the initial phase and in larger intervals later in the course of reaction.

Stopped-Flow Kinetics. Fast unfolding experiments (half times <1 s) were performed with the π*-180 instrument (Applied Photophysics, Ltd.). Dead time was 1−2 ms; the optical path was 1 cm; the slits were set to 4 nm; and the detection wavelength was 225 nm. Unfolding was triggered by rapid mixing of protein solution in PBS with a buffer containing various concentrations of GdmCl at a mixing ratio of 1:10 and a flow rate of 5 mL s^{-1}. The final protein concentration was 5.4 μM (monomer equivalents), and the GdmCl concentrations varied between 4.53 and 5.45 M. At least three kinetic traces were averaged and used for further analysis.

Data Analysis. Equilibrium and kinetic data were analyzed according to the two-state-model assuming the presence of only the fully folded trimer (T) and the fully unfolded monomer (M) at each GdmCl concentration (*6*). The corresponding reaction scheme is as follows:

$$T \underset{k_f}{\overset{k_u}{\rightleftharpoons}} 3M$$

where k_u and k_f are the microscopic rate constants for unfolding and refolding, respectively. The unfolding equilibrium constant is defined in the usual way as $K_U = k_u/k_f$ and is related to the free energy change by $\Delta G = -RT \ln K_U$. For a given total concentration of the folded trimer, C_T, and defining f_U as the molar fraction of the unfolded protein (monomer), K_U is expressed by

$$K_U = \frac{27 f_U^{\,3} C_T^{\,2}}{1 - f_U} \quad (1)$$

f_U is calculated from the only real solution of eq 1

$$f_U = \sqrt[3]{A} - \frac{1}{3}\frac{k}{A} \quad (2)$$

where

$$k = \frac{K_U}{27 C_T} \text{ and } A = k\left(\frac{1}{2} + \frac{\sqrt{3}\sqrt{4k + 27}}{18}\right)$$

The equilibrium unfolding data were analyzed by the linear extrapolation method (LEM) using an in-house written script for Mathematica (Wolfram Research, Inc.) for nonlinear least-squares optimization of the values for ΔG_U in the absence of the denaturant and $m_{eq} = d\Delta G_U/d[\text{GdmCl}]$ as described elsewhere (*6*). The midpoint of denaturation, $[\text{GdmCl}]_{1/2}$ was calculated from the maximum of the first derivative of the $df_U/d[\text{GdmCl}]$ function.

Kinetic traces were analyzed by the numerical integration of the following equations:

$$\frac{d[M]}{dt} = -3k_f[M]^3 + 3k_u[T] \quad (3a)$$

$$\frac{d[T]}{dt} = k_f[M]^3 - k_u[T] \quad (3b)$$

Modeling according to a more complicated mechanism assuming the presence of a dimeric intermediate indicated a negligible fractional population of the dimer (less than 1%) and led to no improvement of the fitting statistics. If the simple two-state folding/unfolding mechanism is correct, the microscopic rates constants of folding and unfolding are expected to change exponentially with denaturant concentration according to the following equations:

$$\ln k_f = \ln k_f^{H_2O} + m_f[\text{GdmCl}] \quad (4a)$$

$$\ln k_u = \ln k_u^{H_2O} + m_u[\text{GdmCl}] \quad (4b)$$

The superscript H_2O refers to the rate constants in the absence of the denaturant, and m_f and m_u (in units of M^{-1}) describe the linear dependence of ln k_f and ln k_u on the denaturant concentration, respectively.

Numerical Simulations. Eqs 3a and 3b were used to simulate the time-dependent changes in the concentrations of the trimer and monomer in different GdmCl concentrations. The rate constants were calculated by interpolation of the functions given by eqs 4a and 4b and representing best fits to the experimental data (straight lines in Figure 4). The folding reactions were simulated starting with [M] = 12 μM, and the unfolding reactions were simulated with [T] = 4 μM so that at infinite time the simulated fractional population of M and T at each GdmCl concentration should correspond to the fractional population of M and T observed in the equilibrium unfolding experiment, if the two-state character of folding/unfolding holds for Lpp-56. From the simulations, f_U was calculated as [M]/3[T].

RESULTS

The Lpp-56 protein is a stable trimer in solution (*3*). The mean residue ellipticity at 225 nm (MRE_{225}) in the micromolar concentration range is $\sim -34\,000$ deg cm^2 dmol^{-1}, indicating almost 100% helical content. The apparent midpoint of thermal denaturation is highly dependent on the scanning rate, and only a fraction of the helical signal is regained after fast cooling. However, if the same sample is incubated for prolonged times at 4 °C, MRE_{225} reaches ~90−95% of the initial value. These observations suggest, as has been reported earlier (*4*), that the thermal unfolding reaction is far from equilibrium during heating at experimentally accessible heating rates (down to 0.1 °C min^{-1}). Therefore, it is impossible to extract equilibrium thermodynamic parameters on Lpp-56 unfolding from thermal melting experiments.

Isothermal Solvent-Induced Denaturation. The thermodynamic stability of Lpp-56 was assessed at 4 °C by GdmCl-induced denaturation in PBS at pH 7. This temperature was selected for two reasons. First, Lpp-56 refolding exhibits anti-Arrhenius behavior, the refolding half times decreasing between 4 and 25 °C approximately by a factor of 10 (see Supporting Information). Second, the low-temperature minimizes the chance for bacterial contamination during the long incubation time. The conformational transitions were followed by monitoring MRE_{225}. The experiment was designed in the following way. The fully unfolded protein in 6 M GdmCl was diluted to a final 12 μM concentration (monomer equivalents) in PBS containing increasing amounts of the denaturant. Another series of samples was prepared by transferring the fully folded protein into PBS containing the desired final GdmCl concentration. After 18 h of incubation at 4 °C, the unfolding curves obtained from the two sets of samples were remarkably different (Figure 1). Although MRE_{225} at very low (below 0.4 M) and high (above 4 M) GdmCl were the same, the GdmCl concentrations where the protein was apparently half unfolded differed by almost 2 M. It follows that the equilibration between the folded trimer and the unfolded monomer is unusually slow not only at high temperatures but also at low temperatures in the presence of denaturant. The samples were incubated at 4 °C, and MRE_{225} was remeasured at time intervals until no further signal changes could be detected. This was the case around day 270 of incubation. An additional measurement was

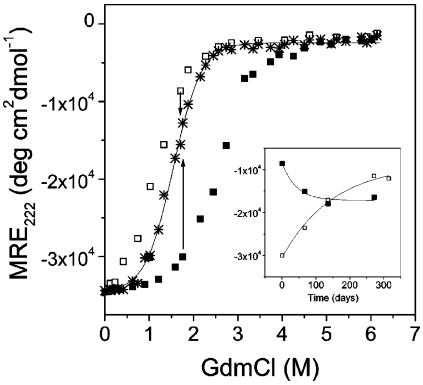

FIGURE 1: Equilibrium isothermal unfolding of Lpp-56 induced by GdmCl at 4 °C. Total protein concentration was 12 μM (monomer equivalents). The squares represent the MRE_{225} measured after 18 h of incubation. Fully unfolded protein in 6 M GdmCl (open symbols) or folded protein in PBS (filled symbols) was diluted to the indicated final denaturant concentrations. MRE_{225} was remeasured at time intervals, and the arrows indicate how the initial apparent unfolding curves converged after prolonged incubation. The asterisks represent MRE_{225} after equilibrium has been reached (after ~270 days of incubation). The continuous line was computed by nonlinear least-squares fitting, assuming a two-state equilibrium between the folded trimer and the unfolded monomer. The data are best described by the following parameters: $[GdmCl]_{1/2}$, = 1.5 ± 0.1 M; $\Delta G^{H_2O}_{U,eq}$ = 79 ± 10 kJ mol^{-1}; m_{eq} = 14.9 ± 2.5 kJ mol^{-1} M^{-1}. Inset: The time course of MRE_{225} changes recorded in 1.7 M GdmCl.

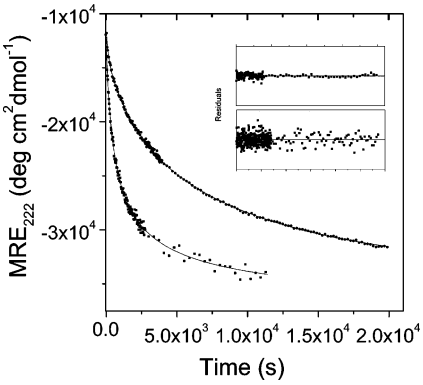

FIGURE 2: Refolding of Lpp-56. The time course of MRE_{225} changes at 4 °C was followed after the rapid transfer of the completely unfolded protein to folding environment. Two representative kinetic traces collected at strong folding conditions are shown. Left trace: temperature jump from 80 °C to 4 °C. Final protein concentration was 24.7 μM (monomer equivalents). Right trace: hundred-fold dilution of Lpp-56 stock solution prepared in 6 M GdmCl and equilibrated at 4 °C. The final protein concentration was 11.2 μM (monomer equivalents), and the final GdmCl concentration was 0.06 M. The continuous lines are best fits according to the ternary reaction by numerical integration of eqs 3a and 3b. The residuals of the fits are shown in the inset.

performed at day 300 of incubation to verify the constancy of the signal. As seen in Figure 1, the ellipticity of the samples from the two sets of experiments at the same GdmCl concentration slowly converged over time. All data points were combined to calculate the stability of Lpp-56. The resulting unfolding curve could be reasonably described by a simple two-state unfolding of the folded trimer to the unfolded monomer. The free energy of unfolding at 4 °C, $\Delta G^{H_2O}_{U,eq}$, is 79 ± 10 kJ mol^{-1}. The midpoint of the unfolding transition, $[GdmCl]_{1/2}$, is 1.5 ± 0.1 M, and the dependence of ΔG_{unf} on the concentration of GdmCl, m_{eq}, is 14.9 ± 2.5 kJ mol^{-1} M^{-1} (Table 1).

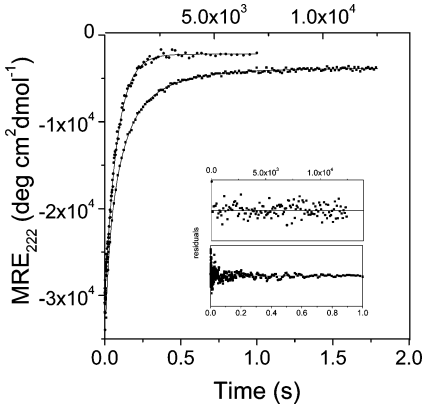

FIGURE 3: Unfolding of Lpp-56; time course of MRE_{225} changes at 4° C after the rapid dilution of folded protein into a GdmCl-containing buffer. Upper trace and lower *x*-axis: unfolding in 5.45 M GdmCl measured by CD stopped-flow. The final protein concentration was 5.4 μM (monomer equivalents). Lower trace and upper *x*-axis: unfolding in 3.25 M GdmCl. The experiment was performed by manual mixing using a conventional CD spectropolarimeter. The final protein concentration was 31 μM (monomer equivalents). The continuous lines are best fits according to the ternary reaction by numerical integration of eqs 3a and 3b. The residuals of the fits are shown in the inset.

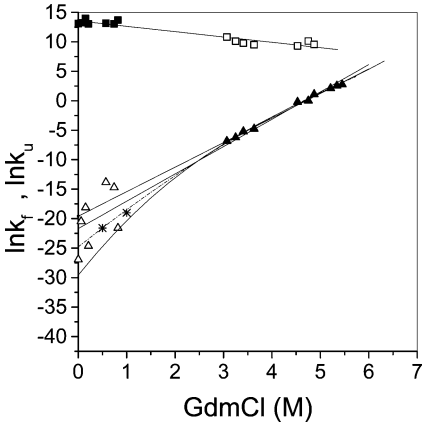

FIGURE 4: GdmCl dependence of the rate constants for refolding (■, □) and unfolding (▲, △). The rate constants k_f and k_u were calculated from the numerical integration of eqs 3a and 3b. The filled symbols represent data obtained at strong folding (<1 M GdmCl) and strong unfolding (>3 M GdmCl) conditions. Unfolding data were collected by manual mixing (3−4 M GdmCl) and by a CD stopped flow (>4.5 M GdmCl). The open symbols represent the natural logarithm of rate constants for unfolding and refolding extracted from analysis of kinetic traces, which were recorded at GdmCl concentrations where refolding and unfolding are dominating. Continuous lines are linear fits according to eqs 4a and 4b. All refolding data are best described with $k_f^{H_2O}$ = (7.6 ± 1.5) × 10^5 M^{-2} s^{-1} and m_f = 0.91 ± 0.08 M^{-1}. The upper line associated with unfolding data was calculated considering only data collected at strong unfolding conditions ($k_u^{H_2O}$ = (3.1 ± 1.0) × 10^{-9} s^{-1}; m_u = 4.16 ± 0.11 M^{-1}). The lower line describes all unfolding data ($k_u^{H_2O}$ = (3.8 ± 3.0) × 10^{-10} s^{-1}; m_u = 4.63 ± 0.50 M^{-1}). The asterisks are the natural logarithm of rate constants, which, according to numerical simulations, would explain the deviation between the equilibrium and kinetic data below ~1.2 M GdmCl (see Results and Figure 5 for details). The dotted line is a function smoothly connecting the simulated data with the directly measured data in the unfolding region. The intercept at 0 M GdmCl predicts $k_u^{H_2O}$ = 2 × 10^{-11} s^{-1}. The lowest continuous line illustrates a hypothetical dependence of ln k_u on [GdmCl]. Details are given in the text.

Folding/Unfolding Kinetics. The kinetic behavior of the Lpp-56 protein was studied at 4 °C by following the time

Table 1: Equilibrium and Kinetic Parameters Describing Folding of Lpp-56[a]

equilibrium parameters	kinetic parameters
$[GdmCl]_{1/2}$[b]	$k_f^{H_2O} \times 10^{-5}$
1.5 ± 0.1	6.3 ± 1.5[c]
	6.6 ± 0.8[d]
	7.6 ± 1.5[e,f]
	average
	6.8 ± 2.3
	$k_u^{H_2O} \times 10^{9}$
	3.10 ± 1.00[f,g]
	0.38 ± 0.30[f,h]
	0.02 ± 0.02[i]
	~ 0.0001[j]
	m_f
	-0.91 ± 0.08[f]
	m_u
	4.16 ± 0.11[f,g]
	4.63 ± 0.50[f,h]
$\Delta G_{U,eq}^{H_2O}$[b]	$\Delta G_{U,kin}^{H_2O}$[k]
79 ± 10	76 ± 15[g]
	81 ± 20[h]
	88 ± 20[i]
	~ 100[j]
m_{eq}[b]	m_{kin}[l]
14.9 ± 2.5	11.7 ± 0.2[g]
	12.7 ± 0.5[h]

[a] In PBS at pH 7 and 4 °C. $[GdmCl]_{1/2}$ in units of M; $k_f^{H_2O}$ in units of M^{-2} s^{-1}; $k_u^{H_2O}$ in units of s^{-1}; m_f and m_u in units of M^{-1}; $\Delta G_U^{H_2O}$ in units of kJ mol^{-1}; m_{eq} and m_{kin} in units of kJ mol^{-1} M^{-1}. [b] The parameters obtained by nonlinear optimization of a two-state model to the data (*6*). [c] Refolding in plain buffer; the mean of three experiments. [d] The mean of rate constants measured in 0−0.82 M GdmCl. [e] The linear fitting of data between 0 and 5.2 M GdmCl. [f] The parameters obtained by the linear fitting of eqs 4a or 4b. [g] The linear fitting of data between 3 and 5.5 M GdmCl. [h] The linear fitting of data between 0 and 5.5 M GdmCl. [i] With simulated curvature below 1 M GdmCl; dotted line in Figure 4. [j] Estimated upper limit (see text for details). [k] Calculated according to $\Delta G_U = -RT \ln(k_u/k_f)$. [l] Calculated according to $m_{kin} = RT(|m_f| + |m_u|)$.

course of the MRE_{225} change accompanying the formation/disruption of the helical structure. Figures 2 and 3 illustrate representative refolding and unfolding experiments. All kinetic traces were well reproduced when solving the differential equations describing the ternary monomer-to-trimer reaction (eqs 3a and 3b). Because the apparent refolding half times are long in the low-micromolar range of protein concentrations, refolding kinetic experiments could be performed at strong folding conditions (subdenaturing, 0−1 M GdmCl concentrations). Refolding was initiated either from the heat denatured state or form the chemically denatured state in 6 M GdmCl. The refolding rate constant measured in plain buffer is $k_f^{H_2O} = (6.3 \pm 1.5) \times 10^5$ M^{-2} s^{-1}. Within error, k_f was independent of the GdmCl concentration below 1 M ($m_f = d\ln k_f/d[GdmCl] = -0.004 \pm 0.45$ M^{-1}). The average value of $k_f^{H_2O}$ from all 9 experiments is $(6.6 \pm 0.8) \times 10^5$ M^{-2} s^{-1}. Still another estimate of $k_f^{H_2O}$ can be obtained if one assumes that the linear dependence of the refolding rate constant on the denaturant concentration holds in a broad range of [GdmCl] and considers k_f values obtained from the analysis of unfolding traces collected at strong denaturing conditions ([GdmCl] >3 M; Figure 4). Although, the fitting values of k_f in unfolding experiments are statistically underdetermined, the whole set of 16 data points can be reasonably described by a straight line ($R^2 = 0.913$). Extrapolation to 0 M GdmCl yields $k_f^{H_2O} = (7.6 \pm 1.5) \times 10^5$ M^{-2} s^{-1}. Considering the stated errors, all three values agree well, and their average is $(6.8 \pm 2.3) \times 10^5$ M^{-2} s^{-1}. From the slope of the straight line shown in Figure 4, one calculates $m_f = -0.91 \pm 0.08$ M^{-1}.

The rates of unfolding were measured either in the stopped-flow instrument or by manual dilution of the folded protein into buffer containing increasing GdmCl concentrations (Figure 3). Both sets of data fit very well to each other and describe an exponential increase of the unfolding half times with increasing denaturant concentration in the tested range (Figure 4). The apparent rate constant of unfolding, $k_u^{H_2O}$, was estimated in two ways. The data collected at [GdmCl] >3 M are consistent with linear eq 4b ($R^2 = 0.994$), from which we calculate $k_u^{H_2O} = (3.1 \pm 1.0) \times 10^{-9}$ s^{-1} and $m_u = d\ln k_u/d[GdmCl] = 4.16 \pm 0.11$ M^{-1}. Because the extrapolation to 0 M GdmCl is a very long one and the assumption of eq 4b might not be generally valid, we assessed k_u values that were calculated as fitting parameters in the numerical analysis of refolding reactions at strong folding conditions according to eq 3a. As seen in Figure 4, and as expected, the confidence in these values is low. They do not exhibit any systematic dependence on [GdmCl] ($R^2 = 0.14$). The best linear fit of all data according to eq 4b results in $k_u^{H_2O} = (3.8 \pm 3.0) \times 10^{-10}$ s^{-1} and $m_u = d\ln k_u/d[GdmCl] = 4.63 \pm 0.50$ M^{-1} ($R^2 = 0.935$).

The calculated rate constants for refolding and unfolding are listed in Table 1. From kinetic data, the free energy of unfolding at 4 °C, $\Delta G_{U,kin} = -RT \ln(k_u^{H_2O}/k_f^{H_2O})$, is 76 ± 15 and 81 ± 20 kJ mol^{-1}, $m_{kin} = RT(|m_f| + |m_u|)$ is 11.7 ± 0.2 and 12.7 ± 0.5 kJ mol^{-1} M^{-1}, depending on which estimate of $k_u^{H_2O}$ and m_u is used in the calculation. Although the errors are large, the correspondence between parameters derived from independent equilibrium and kinetic experiments is very good. Assuming simple refolding/unfolding kinetics and using the kinetic parameters from Table 1, one can calculate k_f and k_u and simulate the expected equilibrium concentrations of the folded trimer and the unfolded monomer at any GdmCl concentration. Figure 5 illustrates the overall similarity between the unfolding curve measured at equilibrium and the one derived from kinetic experiments. However, a closer inspection reveals that the extent of unfolding that is predicted from the linear extrapolation of k_u is larger than that measured in equilibrium below approximately 1 M GdmCl. Numerical simulations demonstrate that the correspondence between equilibrium and kinetic data is significantly improved if one assumes a downward concave curvature of the ln k_u versus [GdmCl] plot (asterisks and dotted line in Figure 4).

DISCUSSION

We have measured the stability and the kinetic behavior of the trimeric coiled-coil core of the *E. coli* outer membrane lipoprotein (Lpp-56). Because both refolding and unfolding are slow in comparison to those in many other proteins studied to date, estimating the thermodynamic stability and the rates of formation and disruption of the native structure is not a trivial task. Because of the almost complete kinetic

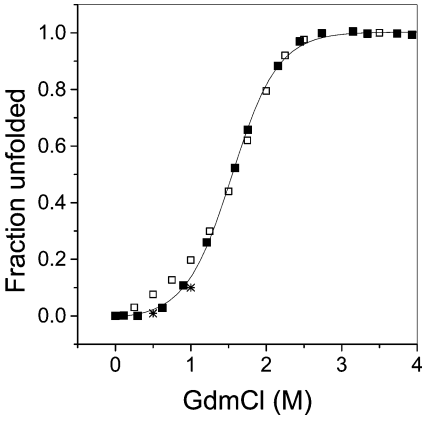

FIGURE 5: GdmCl dependence of the equilibrium distribution between the folded trimer and the unfolded monomer. The filled symbols represent the fraction of unfolded Lpp-56 calculated from the equilibrium unfolding experiment (see Figure 1). Open symbols are the results of numerical simulations according to eqs 3a and 3b as described in Experimental Procedures. The asterisks are f_U values calculated from simulations in which k_f were taken from the best linear fit of eq 4a to the folding data in Figure 4, whereas k_u values were set to 5.6×10^{-9} s^{-1} (0.5 M GdmCl) and 4×10^{-10} s^{-1} (1 M Gdm), instead of 4×10^{-9} s^{-1} and 3.9×10^{-9} s^{-1}, respectively, which correspond to the best linear fit of eq 4b to the unfolding data in Figure 4.

irreversibility, the application of the van't Hoff formalism to extract thermodynamic information from spectroscopic and calorimetric thermal unfolding data is impossible (*4*). We assessed the stability of Lpp-56 at low temperature by using GdmCl as the denaturing agent. ΔG_U of unfolding was calculated by the standard linear extrapolation method (LEM) in the limit of equilibrium two-state folding/unfolding transition. In view of the known kinetic peculiarity of the protein, the approach requires justification. In a reversible process, the same partitioning of molecular species is expected at equilibrium, regardless of the initial state of the system. This was indeed the case with Lpp-56. At each GdmCl concentration, MRE_{225} converged to the same value (within the error of concentration determination and instrumental noise) if equilibration was attained starting either from the fully denatured state or from the fully folded state. As to the validity of the two-state approximation, the presence of intermediate states cannot be completely ruled out on the sole basis of denaturant-induced unfolding data. For example, the observed ellipticity in the transition region could contain contribution from intermediates with partially developed helical structure. However, the unfolding curve shown in Figure 1 is symmetrical around the midpoint of unfolding and exhibits no detectable kinks. It is unlikely that the population of major intermediates would shift smoothly with the variation in GdmCl concentration. Alternatively, intermediates without helical structure might escape detection by CD spectroscopy. Because the Lpp-56 monomers are unstructured in isolation and the folded trimer is stabilized by nonpolar contacts at the interface between the helices, the presence of nonhelical, sufficiently stable states appears very improbable. Light scattering experiments in aqueous solutions at higher temperatures failed to detect dimeric intermediates (*4*). A strong argument in favor of the validity of the two-state approximation comes from kinetic data. The refolding and unfolding traces can be modeled with simple trimolecular refolding and unimolecular unfolding reactions, respectively. The limbs of the chevron plot shown in Figure 4 are reasonably linear. There is a very good agreement between ΔG_U and m values calculated from equilibrium and kinetic data (Table 1) as well as between unfolding curves derived from equilibrium and kinetic data (Figure 5).

There are two published studies dealing with the thermodynamic stability of Lpp-56. Shu et al. estimated the unfolding free energy as 86 kJ mol^{-1} from GdmCl denaturation (*3*). However, this number was derived at nonequilibrium conditions and, therefore, does not reflect the true free energy change of unfolding. The numerical similarity between ΔG_U obtained in ref 3 (*3*) and that in our study is perhaps a fortuitous event. More recently, DP suggested that the genuine thermodynamic stability of Lpp-56 at 4 °C is much higher, on the order of 140 kJ mol^{-1} (*4*). The difference between the latter number and our own estimate of ~80 kJ mol^{-1} is striking. Both analyses are based on the two-state model of unfolding. It must be noted, however, that the two studies differ in one fundamental aspect. DP used heat, whereas we used GdmCl to induce a shift of the conformational equilibrium between the native and the denatured state and modulate the rates of folding and unfolding. Heat and chemical denaturants have been widely used to examine the energetics of proteins, but the physical origin of their action as denaturing agents is quite different. Discrepancies between ΔG_U derived from thermal and chemical denaturation are documented (*7*−*10*). The applicability and pitfalls of LEM as a tool to quantify protein stability have been discussed from theoretical and experimental points of view (*11*−*14*).

The height of the activation barrier for folding, $\Delta G_{‡-D}$, is rigorously defined because the refolding rate was measured directly in benign buffer at low temperature, and we, along with DP, obtained very similar values for k_f. Moreover, the folding rate variation upon increasing the GdmCl concentration and increasing the temperature is relatively weak (Figure 4 in this article, and Figure 5 in ref 4 (*4*)). Given that the two-state model of Lpp-56 unfolding holds reasonably well for both thermal- and denaturant-induced unfolding, the disparity in ΔG_U values has to be attributed to different heights of the unfolding activation barrier, $\Delta G_{‡-N}$, which was estimated using long extrapolation. Indeed, k_u was directly measured only at strong unfolding conditions between 3 and 5.5 M GdmCl and between 60 and 70 °C. In principle, the linearity of ln k_u versus [GdmCl] or ln k_u versus $1/T$ plots would indicate that $\Delta G_{‡-N}$, that is, the energetic difference between the native and the transition state, changes smoothly over the considered range of denaturant concentrations or temperatures. However, linearity outside the experimentally accessible range of solvent conditions is not granted a priori. As demonstrated in Figures 4 and 5, the data indicate a possible downward concave curvature of the ln k_u versus [GdmCl] plot (asterisks and dotted line in Figure 4).

Among alternatives, the simplest and perhaps the most intuitive explanation for the predicted deviation from linearity comes from considering electrostatic effects. GdmCl is a salt and attenuates electrostatic interactions by screening the Coulombic attraction between opposite charges and/or by altering the desolvation contributions to the total electrostatic free energy. The effect is concentration-dependent, implying that a pronounced change of the electrostatic component of ΔG_U is expected between 0 and 1 M GdmCl, at which salt concentration, charge−charge interactions are usually as-

sumed to be insignificant. If the native state is stabilized by electrostatics, the addition of salt will increase its free energy and, therefore, $\Delta G_{\ddagger-N}$ will abruptly decrease between 0 and 1 M, yet linear extrapolation from much higher GdmCl concentrations will fail to detect the effect. Alternatively, GdmCl might stabilize the transition state by abolishing unfavorable electrostatic interactions (or in some other way). In view of the very weak variation of k_f between 0 and 1 M GdmCl (Figure 4), we render this possibility unlikely.

Indeed, electrostatic effects appear to be an important factor governing the the conformational stability of Lpp-56. There are close ionic contacts seen in the crystal structure, some of them forming salt bridge networks (*3*). DP convincingly demonstrated that the stability of Lpp-56 is much lower at pH 3, where at least most of the salt bridges are disrupted. In fact, ΔG_U at pH 3 is almost half of that at neutral pH according to their estimate and is very close to what we have found. We are currently investigating the electrostatic contribution to Lpp-56 stability by computational methods. In the following, we argue, however, that the lower ΔG measured by GdmCl-induced unfolding cannot be entirely explained by the electrostatic effect of GdmCl.[2]

Charge screening (or other attenuation of electrostatics) by GdmCl is expected to induce a steep decrease of $|m_{kin}|$ (and $|m_{eq}|$) between 0 and 1 M denaturant. Because $m_{kin} = RT(|m_f| + |m_u|)$ and the dependence of $\ln k_f$ on GdmCl, m_f, is quite small (see Figure 4), it is m_u that largely accounts for the experimentally observed m_{kin}. It follows that a pronounced downward curvature of the $\ln k_u$ versus [GdmCl] plot will result. An arbitrarily drawn $\ln k_u$ dependence is shown in Figure 4 (lowest continuous line). It smoothly deviates from linearity below ~1.5 M GdmCl. The actual curvature of this function is indeed not known, yet there are two important constraints. First, the deviation from linearity is very unlikely to be pronounced above 1−1.5 M GdmCl (*8*, *9*, *15*, *16*). Second, the slope around 0 M GdmCl cannot exceed some limiting value because $|m_u| \leq m_{eq}/RT - |m_f|$. Setting $m_f = 0$, this limit is given by some physically reasonable m_{eq} value. For a protein of the size of Lpp-56, the expected m value is on the order of 20−25 kJ mol^{-1} M^{-1}, if unfolding is complete (*13*), and therefore, $|m_u|$ cannot exceed 9−11 M^{-1}. The line shown in Figure 4 was drawn with $|m_u| = 10$ M^{-1} between 0 and 1 M GdmCl. The exercise leads to the conclusion that the true unfolding rate constant in the absence of GdmCl is on the order of 10^{-13} s^{-1} as a limit, implying that genuine Lpp-56 stability is on the order of 100 kJ^{-1} mol^{-1}. Hence, the linear extrapolation procedure underestimates the Lpp-56 stability by 10−20 kJ mol^{-1}. The differences in protein stability (including the stability of coiled coils) calculated from GdmCl or urea/thermal unfolding have been invariably estimated in the range 5−15 kJ mol^{-1} (*7*−*10*, *15*, *17*−*20*).

The above discussion does not intend to invalidate the experimental results of DP in any way. It only illustrates that arguments based solely on salt effects seems not to reconcile the ΔG_U that we found from chemical unfolding with that found by DP from thermal unfolding. The two studies provide contradictory views about the nature of the transition state as well. DP found the main change in ΔC_p to occur between the unfolded monomeric state and the transition state, whereas the heat capacity difference between the native trimer and the transition state is negligible. As far as the ΔC_p of the protein, conformational changes are mostly caused by changes in the hydration of apolar groups, this observation suggests high structural similarity between the native and transition states. In contrast, we found that Lpp-56 traverses an unstructured and highly solvent-accessible high energy state. This follows from the very low Tanford β_T value, which reflects the buried surface area in the transition state relative to the native state. ($\beta_T = 1 - |m_f|/(|m_f + m_u|) \sim 0.15$; see Table 1). The transition state in the folding of short dimeric coiled coils has been found to be either significantly structured or largely unstructured, depending on the experimental approach (*21*−*24*). It has been proposed that the high-temperature transition state moves toward the native state in accord with the Hammond postulate (*25*). It is possible that the structural properties of, and thereby the energetic differences between, the ground states and the activated state vary in different ways with the temperature and denaturant concentration, and thus, different unfolding pathways have been sampled in the two studies.[3]

The role of electrostatic interactions in general and of salt bridges in particular to coiled coil stability has been a subject of controversy for some time. Both stabilization and destabilization by surface-exposed ion pairs have been documented (*18*, *20*, *26*). To our knowledge, there are no cases where salt bridges dominate the structural energetics of coiled coils, which are mainly stabilized by the packing of nonpolar side chains at the interhelical interface. It appears that charge−charge attractions and repulsions are factors that modulate the rate of association-coupled refolding (*27*), assist (and maintain) the in-register alignment and the directionality of the super-helix (*28*), and govern the specificity of oligomerization (*29*). In this respect, our finding that the rate of Lpp-56 refolding is much less affected by the salt nature of GdmCl than the rate of unfolding is surprising. It appears that ionic contacts genuinely stabilize the folded conformation of this trimeric coiled-coil. It must be noted, however, that the term salt bridge is usually employed when referring to the close proximity of two oppositely charged groups. The nonpolar moiety of ionizable side chains might participate in hydrophobic packing as well. This is the case in Lpp-56, where residues occupying the canonical hydrophobic *a* and *d* heptad positions pack not only against each other but also against the charged residues occupying the *e* and *g* positions to complete the hydrophobic core (*3*). Therefore, the disruption of a salt bridge by pH or salt would also alter packing and would lead to an indirect destabilization. Indeed, at pH 3, DP found a significant increase in the temperature

[2] The similarity between ΔG_U measured at pH 3 and ΔG_U measured in GdmCl cannot be taken at face value as representing the same electrostatic effect. The lowering of pH will induce the protonation of acidic groups and thereby will cause the disruption of salt bridges. However, the degree of protonation depends on the actual (and a priori unknown) pK_a values of individual Asp and Glu side chains. Furthermore, the denatured state will be highly positively charged. The situation is different in GdmCl. If, for simplicity, we assume the primary electrostatic effect of GdmCl to be the screening of charge−charge interactions, these interactions will be screened not only in the native state but also in the denatured state.

[3] It is worth noting that ΔC_p (11 J K^{-1} (mol res^{-1})) and m_{eq} (62 J (mol res)$^{-1}$ M^{-1}) for Lpp-56 unfolding are both much lower than the mean values for globular proteins (58 J K^{-1}(mol res^{-1}) and 98 J(mol res)$^{-1}$ M^{-1}, respectively).

dependence of the partial molar heat capacity of native Lpp-56 and a much lower enthalpy and entropy, characterizing the transition from the folded to the activated state.

Why is Lpp-56-folding and refolding so slow? The folding of an oligomeric coiled coil is tightly coupled to the association of polypeptides, which are intrinsically devoid of stable tertiary structure in isolation. For a trimeric coiled coil, the simultaneous association of three chains is very unlikely from a statistical point of view. Furthermore, folding could be slow if the folding mechanism involves the formation of a nucleation site by association of monomeric chains that are partly helical and/or in-register, that is, in the correct orientation allowing structure propagation. The presence of a sequence triggering the folding of dimeric coiled coils has been suggested (*30*−*32*). Interestingly, the AGADIR algorithm predicts for the isolated Lpp-56 chains a 15−25% helical propensity localized in the *C*-terminal stretch encompassing the alanine zipper (Supporting Information). Along the same lines, structure consolidation toward the optimal, in-register alignment of the monomers might involve the sliding of the polypeptide chains within an initial associated state. Of note is the fact that all *a* and *d* positions participating in the Lpp-56 hydrophobic core are occupied by nonpolar residues, whereas most naturally occurring coiled coils contain buried polar residues (*33*). Such polar clusters have been demonstrated to warrant the proper orientation of coiled coil monomers and to govern the dimerization specificity. It is likely that they may also confer a mechanism speeding up folding by providing buoys in the hydrophobic core. Although speculative at present, this suggestion is corroborated by our studies at pH 5. We tested the effect of the replacement of alanine 37 (*d* heptad position) and alanine 41 (*a* heptad position) by polar glutamine. The two variants were more stable in thermal unfolding experiments (apparent T_m shifts of 8 and 10 °C, respectively) and refolded faster than wild-type Lpp-56 by a factor of 10 (Supporting Information).

The very slow unfolding rate is most likely a combination of different factors. Unfolding accompanied by the simultaneous dissociation of the three chains will require the simultaneous disruption of the packing interactions in the extended hydrophobic core, the breakage of (apparently strong) salt bridges, and the opening of the *N*- and *C*-terminal caps. Such a concerted event is expected to occur rather infrequently. The unfolding half times at benign conditions are 10^2−10^5 years (this study) and 10^{12} years (derived from the data of DP). Both numbers are difficult to comprehend. Very slow unfolding is not exceptional, and plausible arguments have been put forward in favor of the existence of evolutionary pressure for increasing the kinetic stability of certain classes of proteins (*34*, *35*). To our knowledge, however, Lpp-56 is the first coiled coil for which a high unfolding kinetic barrier has been experimentally demonstrated.

ACKNOWLEDGMENT

We thank Dr. Min Lu for providing the protein used in this study, Dr. Daniel Nettels for help with Mathematica scripts, and Dr. Christine Berger Sprecher for valuable discussions.

SUPPORTING INFORMATION AVAILABLE

Figures describing thermal unfolding and refolding kinetics of wild-type Lpp-56 and two Ala-to Gln variants at pH 5. This material is available free of charge via the Internet at http://pubs.acs.org

REFERENCES

1. Goodsell, D. S., and Olson, A. J. (1993) Soluble-proteins − size, shape and function, *Trends Biochem. Sci. 18*, 65−68.
2. Lupas, A. N., and Gruber, M. (2005) The structure of alpha-helical coiled coils, *Adv. Protein. Chem. 70*, 37−78.
3. Shu, W., Liu, J., Ji, H., and Lu, M. (2000) Core structure of the outer membrane lipoprotein from *Escherichia coli* at 1.9 A resolution, *J. Mol. Biol. 299*, 1101−1112.
4. Dragan, A. I., Potekhin, S. A., Sivolob, A., Lu, M., and Privalov, P. L. (2004) Kinetics and thermodynamics of the unfolding and refolding of the three-stranded alpha-helical coiled coil, Lpp-56, *Biochemistry 43*, 14891−14900.
5. Edelhoch, H. (1967) Spectroscopic determination of tryptophan and tyrosine in proteins, *Biochemistry 6*, 1948−1954.
6. Marti, D. N., Bjelic, S., Lu, M., Bosshard, H. R., and Jelesarov, I. (2004) Fast folding of the HIV-1 and SIV gp41 six-helix bundles, *J. Mol. Biol. 336*, 1−8.
7. Ferreon, A. C. M., and Bolen, D. W. (2004) Thermodynamics of denaturant-induced unfolding of a protein that exhibits variable two-state denaturation. *Biochemistry 43*, 13357−13369.
8. Ibarra-Molero, B., and Sanchez-Ruiz, J. M. (1996) A model-independent, nonlinear, extrapolationprocedure for the characterization of protein folding energetics from solvent-denaturation data, *Biochemistry 35*, 14689−14702.
9. Makhatadze, G. I. (1999) Thermodynamics of protein interactions with urea and guanidinium hydrochloride, *J. Phys. Chem. B 103*, 4781−4785.
10. Pfeil, W. (2001) *Protein Stability and Folding: A Collection of Thermodynamic Data.*, Springer-Verlag, New York.
11. Alonso, D. O. V., and Dill, K. A. (1991) Solvent denaturation and stabilization of globular proteins, *Biochemistry 30*, 5974−5985.
12. Johnson, C. M., and Fersht, A. R. (1995) Protein stability as a function of denaturant concentration: The thermal-stability of barnase in the presence of urea, *Biochemistry 34*, 6795−6804.
13. Myers, J. K., Pace, C. N., and Scholtz, J. M. (1995) Denaturant m-values and heat-capacity changes: Relation to changes in accessible surface-areas of protein unfolding, *Protein Sci. 4*, 2138−2148.
14. Yao, M., and Bolen, D. W. (1995) How valid are denaturant-induced unfolding free-energy measurements: Level of conformance to common assumptions over an extended range of ribonuclease A stability, *Biochemistry 34*, 3771−3781.
15. Ibarra-Molero, B., Loladze, V. V., Makhatadze, G. I., and Sanchez-Ruiz, J. M. (1999) Thermal versus guanidine-induced unfolding of ubiquitin. An analysis in terms of the contributions from charge−charge interactions to protein stability, *Biochemistry 38*, 8138−8149.
16. Plaxco, K. W., and de los Rios, M. A. (2005) Apparent Debye−Huckel electrostatic effects in the folding of a simple, single domain protein. *Biochemistry 44*, 1243−1250.
17. Bolen, D. W., and Yang, M. (2000) Effects of guanidine hydrochloride on the proton inventory of proteins: Implications on interpretations of protein stability, *Biochemistry 39*, 15208−15216.
18. Monera, O. D., Kay, C. M., and Hodges, R. S. (1994) Protein denaturation with guanidine-hydrochloride or urea provides a different estimate of stability depending on the contributions of electrostatic interactions, *Protein Sci. 3*, 1984−1991.
19. Perez-Jimenez, R., Godoy-Ruiz, R., Ibarra-Molero, B., and Sanchez-Ruiz, J. M. (2004) The efficiency of different salts to screen charge interactions in proteins: A Hofmeister effect? *Biophys. J. 86*, 2414−2429.
20. Phelan, P., Gorfe, A. A., Jelesarov, I., Marti, D. N., Warwicker, J., and Bosshard, H. R. (2002) Salt bridges destabilize a leucine zipper designed for maximized ion pairing between helices, *Biochemistry 41*, 2998−3008.
21. Bhattacharyya, R. P., and Sosnick, T. R. (1999) Viscosity dependence of the folding kinetics of a dimeric and monomeric coiled coil, *Biochemistry 38*, 2601−2609.

22. Bosshard, H. R., Durr, E., Hitz, T., and Jelesarov, I. (2001) Energetics of coiled coil folding: The nature of the transition states, *Biochemistry 40*, 3544−3552.
23. Moran, L. B., Schneider, J. P., Kentsis, A., Reddy, G. A., and Sosnick, T. R. (1999) Transition state heterogeneity in GCN4 coiled coil folding studied by using multisite mutations and crosslinking, *Proc. Natl. Acad. Sci. U.S.A. 96*, 10699−10704.
24. Sosnick, T. R., Jackson, S., Wilk, R. R., Englander, S. W., and DeGrado, W. F. (1996) The role of helix formation in the folding of a fully alpha-helical coiled coil, *Proteins: Struct., Funct., Genet. 24*, 427−432.
25. Otzen, D. E., and Oliveberg, M. (2004) Correspondence between anomalous m- and delta Cp-values in protein folding, *Protein Sci. 13*, 3253−3263.
26. Yu, Y., Monera, O. D., Hodges, R. S., and Privalov, P. L. (1996) Ion pairs significantly stabilize coiled-coils in the absence of electrolyte, *J. Mol. Biol. 255*, 367−372.
27. Wendt, H., Leder, L., Harma, H., Jelesarov, I., Baici, A., and Bosshard, H. R. (1997) Very rapid, ionic strength-dependent association and folding of a heterodimeric leucine zipper, *Biochemistry 36*, 204−213.
28. Monera, O. D., Kay, C. M., and Hodges, R. S. (1994) Electrostatic interactions control the parallel and antiparallel orientation of alpha-helical chains in 2-stranded alpha-helical coiled-coils, *Biochemistry 33*, 3862−3871.
29. Yu, Y. B. (2002) Coiled-coils: Stability, specificity, and drug delivery potential. *Adv. Drug Delivery Rev. 54*, 1113−1129.
30. Kammerer, R. A., Jaravine, V. A., Frank, S., Schulthess, T., Landwehr, R., Lustig, A., Garcia-Echeverria, C., Alexandrescu, A. T., Engel, J., and Steinmetz, M. O. (2001) An intrahelical salt bridge within the trigger site stabilizes the GCN4 leucine zipper, *J. Biol. Chem. 276*, 13685−13688.
31. Steinmetz, M. O., Stock, A., Schulthess, T., Landwehr, R., Lustig, A., Faix, J., Gerisch, G., Aebi, U., and Kammerer, R. A. (1998) A distinct 14 residue site triggers coiled-coil formation in cortexillin I, *EMBO J. 17*, 1883−1891.
32. Zitzewitz, J. A., Ibarra-Molero, B., Fishel, D. R., Terry, K. L., and Matthews, C. R. (2000) Preformed secondary structure drives the association reaction of GCN4-p1, a model coiled-coil system, *J. Mol. Biol. 296*, 1105−1116.
33. Akey, D. L., Malashkevich, V. N., and Kim, P. S. (2001) Buried polar residues in coiled-coil interfaces, *Biochemistry 40*, 6352−6360.
34. del Pino, I. M. P., Ibarra-Molero, B., and Sanchez-Ruiz, J. M. (2000) Lower kinetic limit to protein thermal stability: A proposal regarding protein stability in vivo and its relation with misfolding diseases, *Proteins: Struct., Funct., Genet. 40*, 58−70.
35. Jaswal, S. S., Truhlar, S. M. E., Dill, K. A., and Agard, D. A. (2005) Comprehensive analysis of protein folding activation thermodynamics reveals a universal behavior violated by kinetically stable proteases, *J. Mol. Biol. 347*, 355−366.

BI0608156